

Interpretation of strange hadron production at LHC

M Petran¹, J Letessier², V Petracek³ and J Rafelski¹

¹ Department of Physics, University of Arizona, Tucson, AZ 85719, USA

² Laboratoire de Physique Theorique et Hautes Energies, Universite Paris 6, Paris 75005, France

³ Czech Technical University in Prague, Brehova 7, 115 19 Praha 1, Czech Republic

Abstract. We extend the SHM analysis of hadron production results showing here consistency with the increased experimental data set, stability of the fit with regard to inclusion of finite resonance widths and 2-star hyperon resonances. We present new results on strangeness yield as a function of centrality and present their interpretation in terms of QGP inspired model of strangeness abundance in the hadronizing fireball.

1. Inclusion of new data

We interpret strange soft hadron multiplicity results obtained in Pb–Pb collisions at $\sqrt{s_{NN}} = 2.76$ TeV at CERN Large Hadron Collider (LHC). This contribution extends the more detailed presentation of Ref. [1], whereas Ref. [2] provided the related analysis without data inter- or extrapolation. In the results presented here we can use final data for K_S^0 , Λ , Ξ^\pm and Ω^\pm [3, 4]. Our fit with these results converges to the same set of thermal parameters as in [1].

Considering limited space and in order to rely solely on directly measured and final experimental results we show here as an example the centrality 10%–20% data bin. In the top two result rows of Table 1, we compare the prior with the present results for statistical parameters. As before Λ -abundance is the dominant contributor to the error as is seen also in direct comparison of input and output results shown in Figure 1. Thus in Table 1 the χ_{tot}^2 is found to be greater, yet relatively small given the 9 degrees of freedom.

As seen in the top two rows of results, the differences between these two fits are well within the error. Looking at μ_B , recall that we did constrain the value in Ref. [1] by its centrality dependence. Our present result is the outcome of an unconstrained fit for this centrality. This is

Table 1. Comparison of non-equilibrium SHM model parameter obtained in fit to 10–20% centrality results for Pb–Pb collisions at $\sqrt{s_{NN}} = 2.76$ TeV. See text for discussion.

$\Sigma(1560)$	widths	dV/dy [fm ³]	T [MeV]	μ_B [MeV]	γ_q	γ_s	χ_{tot}^2
reported in [1]		2003 ± 47	138.6	1.23 ± 0.06	1.63 ± 0.01	2.06 ± 0.13	3.943
NO	NO	2033 ± 105	138.6	1.36 ± 7.94	1.63 ± 0.01	2.02 ± 0.08	6.599
NO	YES	1978 ± 488	139.3	1.15 ± 0.97	1.62 ± 0.19	2.00 ± 0.31	5.169
YES	NO	2042 ± 409	138.5	0.49 ± 0.35	1.63 ± 0.15	2.03 ± 0.25	4.766
YES	YES	1976 ± 398	139.2	0.74 ± 0.09	1.62 ± 0.01	2.01 ± 0.14	3.472

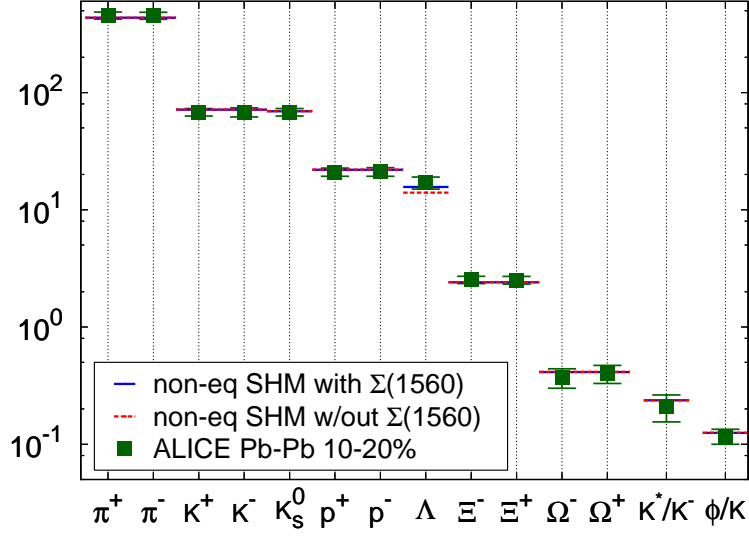


Figure 1. (color online) Comparison of non-equilibrium SHM fit with most recent data from Pb–Pb collisions at $\sqrt{s_{NN}} = 2.76$ TeV for the 10%–20% centrality bin measured by the ALICE collaboration (darkgreen squares), with the 2-star resonance $\Sigma(1560)$ feeding the yield of Λ (solid blue bars), and without the $\Sigma(1560)$ feed (red dashed bars).

possible since the added experimental data for Ξ^\pm and Ω^\pm contain a small particle-antiparticle asymmetry even if this is well within the particle yield error bar. The value of μ_B we find is near to our earlier expectations; however, the error in μ_B is large. There is no error shown for T since the statistical fit error is much smaller than the precision of the result shown. The error that relates directly to the error of fitted particle yields is found to mainly impact dV/dy and γ_s . This shows that there are two types of error in the data: a common normalization error for all data points, and a further strange particle normalization error.

The bulk properties of the fireball at hadronization are shown in Table 2. These are presented without an error estimate: the impact of the error in dV/dy impacts directly the total strangeness yield $N_{s+\bar{s}}$ and entropy S . The other three properties that we show, pressure P , energy density ε , trace anomaly $(\varepsilon - 3P)/T^4$, are impacted by other statistical parameters but the error of γ_s is the most important. The two top rows are practically equal showing that the additional data, and changes in final data do not impact any of the results and discussion presented in Ref. [1].

2. Improving the fit

2.1. Influence of hadron resonance width

The SHARE package [6, 7] was developed with the option of allowing the resonance widths presented by the Particle Data Group [5] (PDG) values. The computing time required to allow the resonance widths is significant with fits needing often more than 24h CPU time. The reason for this is that many numerical foldings need to be performed in order to evaluate the total particle yields; see [6] for details. In the past the small change in outcome did not justify the numerical effort. Thus this test has not been performed often.

The third result row in Table 1 shows the statistical parameters obtained allowing for hadron resonance widths. While χ^2_{tot} of the fit slightly decreases and central points of statistical parameters aside of T agree within error, we note that the error is now more distributed among parameters and the progression is larger indicating slightly less consistency between fit and data.

The fact that there is an increase in T by $\delta T = 0.7$ MeV, which is well above statistical error,

is not surprising considering the systematic effect that the resonance widths have on particle yields. Note that to compensate the increase in value of T the central value of dV/dy decreased. Another consequence of the slight increase of T is a slight (1%) increase of the intensive bulk properties P , ε , $(\varepsilon - 3P)/T^4$, see the third result row in Table 2. The extensive bulk properties directly related to the measured particle yields i.e. $N_{s+\bar{s}}$ and S remain unchanged.

2.2. $\Sigma(1560)$ as a source of Λ

The only data point that is not fitted within the 1 s.d. experimental error margin is the yield of Λ . This situation was also discussed in Ref. [1], where the preliminary Λ/π ratio was fitted and was systematically under-predicted for all centralities as the only data point standing out with model value just outside the one standard deviation error margin. The newly reported experimental value for 10–20% centrality, $\Lambda = 17 \pm 2$, is to be compared to the fitted value, $\Lambda = 14$. Inclusion of hadron resonances with their widths discussed above does not improve the fit to the Λ data point.

The question arises if perhaps a contribution to the Λ yield was inadvertently omitted. The SHARE implementation of SHM [6, 7] includes 3-star (***) and 4-star (****) hadron resonances from among all resonances reported by PDG [5]. There are many omitted 2-star (**) resonances. Generally these are so massive that their contribution to particle yields is insignificant. However, we found one exception to this rule, a $\Sigma(1560)$ which decays into Λ and which would thus systematically increase the Λ yield within the error across all centrality.

The charged states $\Sigma(1560)^\pm$ have been clearly observed (6σ signal) by two independent experiments [8]. On the other hand, no evidence of $\Sigma(1560)^0 \rightarrow \Lambda\pi^0$ has been found in a recent crystal ball experiment [9] and hence the resonance remains unconfirmed at (**) level. $\Sigma(1560)$ quantum numbers have not been measured. Inspired by the close in mass resonance $\Sigma(1580)\frac{3}{2}^-$ [10], we assign spin $\frac{3}{2}$ also to $\Sigma(1560)$.

Once we include $\Sigma(1560)$ in the list of hadron states, the new resonance decay feeds the Λ yield by $\Sigma(1560) \rightarrow \Lambda\pi$ (100%) decay. When we repeat the fit, the resulting statistical model parameters are all almost identical to those without $\Sigma(1560)$ as is seen in Table 1. This means that the other 13 data points alone constrain enough the fit parameters so that the effect of an omitted resonance simply reduces the χ^2 without changing other results. This result confirms ‘missing’ resonance hypothesis as the probable origin of the Λ yield underprediction.

In the final result row in Table 1, we consider the finite width of all resonances and the influence of the 2-star $\Sigma(1560)$ resonance. The overall χ^2_{tot} is decreased by a factor of two, the fitted value of μ_B is showing a relatively small error. The main fit error is in overall normalization dV/dy . The physical bulk properties remain as already obtained and discussed without $\Sigma(1560)$.

Table 2. Comparison of models (see table 1 for all other details) in terms of physical bulk properties. From left to right, we show pressure P , energy density ε , trace anomaly $\varepsilon - 3P$ in units of T^4 , total strangeness $N_{s+\bar{s}}$ and entropy S .

$\Sigma(1560)$	widths	P [MeV/fm ³]	ε [GeV/fm ³]	$(\varepsilon - 3P)/T^4$	$N_{s+\bar{s}}$	S
reported in [1]		79.1	0.467	4.77	384	6466
NO	NO	79.2	0.468	4.79	388	6589
NO	YES	82.0	0.483	4.85	385	6593
YES	NO	78.7	0.465	4.78	387	6574
YES	YES	81.7	0.481	4.84	384	6570

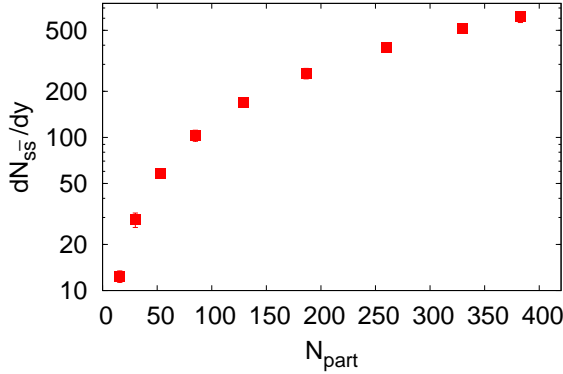


Figure 2. (color online) Total strangeness $dN_{s+\bar{s}}/dy$ produced in Pb–Pb collisions at $\sqrt{s_{NN}} = 2.76$ TeV as a function of centrality.

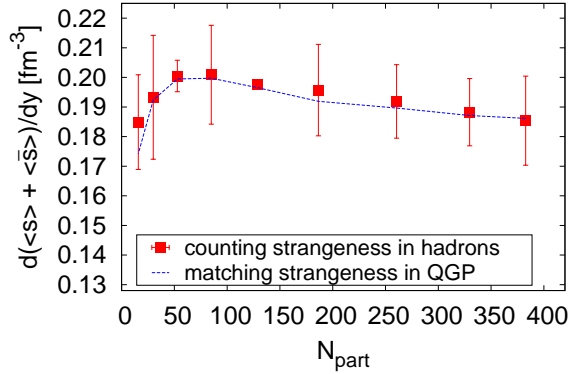


Figure 3. (color online) $s + \bar{s}$ strangeness density per unit rapidity in the hadron phase (red squares), fitted with strangeness in the QGP phase (blue dashed line). See text.

3. Strangeness conservation and strange quark mass at hadronization

In the central Pb–Pb collisions at the LHC, an unprecedented amount of strangeness is produced, a total of $dN_{s\bar{s}}/dy \simeq 600$ strange and anti-strange quarks per unit of rapidity for the most head-on 5% central collisions, see Figure 2. For the peripheral collisions the rise of the total strangeness yield is very rapid, as both the size of the volume and saturation of strangeness production combine. For the more head-on collisions we see a power (~ 1.17) law rise similar to particle interpolation in [1]. Normalization error bar contained in dV/dy is typically 10% is not shown, only the error from γ_s is shown in Figure 2 (often hidden in the symbol size).

The corresponding total observed strangeness density in the hadron phase is depicted in Figure 3. The uncertainty is evaluated using the relative uncertainty of the model parameter γ_s reported in [1]. Note that the variation in density shown is only about $\pm 3.5\%$. Such constancy of the strangeness yield, assuming a recombinant hadronization, should result in strange hadron yield ratios independent of centrality. In Figure 4 the flat line at the bottom is a ratio of two doubly strange particle yields, Ξ/ϕ . Its constancy provides a reference of precision of the argument as this result should be constant [12] even if the strangeness density varies.

The other ratios compare the yield of doubly strange particles with the yield of single strange particles and in one case doubly strange with pions. When strangeness is not saturated as a function of centrality in QGP, one expects an increase in these ratios which we clearly see at lower SPS and RHIC energies. However at LHC a different pattern emerges: there is a bit of increase looking at some of the most peripheral bins which is followed by a slow decrease. The strangeness density shown in Figure 3 mirrors this behavior.

It is of considerable interest to understand if the ‘measured’ strangeness density seen in Figure 3 can be interpreted in terms of sudden hadronization of a QGP fireball. Sudden hadronization implies the conservation of strangeness yield. In sudden hadronization model the volume does not change thus the density in the hadron phase equals that in QGP as well. The chemical freeze-out temperature T is also the hadronization temperature, i.e. the temperature of QGP breakup. We evaluate the QGP phase strangeness density for a given T given by integral of Fermi gas strangeness density in the QGP using [11]:

$$s(m_s, T; \gamma_s^{\text{QGP}}) = -\frac{g}{2\pi^2} \left(\frac{T}{\hbar c}\right)^3 \sum_{n=1}^{\infty} (-\gamma_s^{\text{QGP}})^n \frac{1}{n^3} \left(\frac{nm_s}{T}\right)^2 K_2\left(\frac{nm_s}{T}\right), \quad (1)$$

where m_s is the strange quark mass, γ_s^{QGP} is the phase space occupancy: here superscript QGP

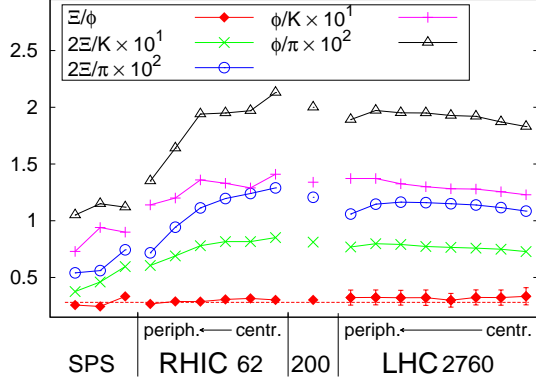


Figure 4. Measured particle ratios from relativistic heavy ion collisions across different collisional energies at SPS, RHIC and LHC, and centralities.

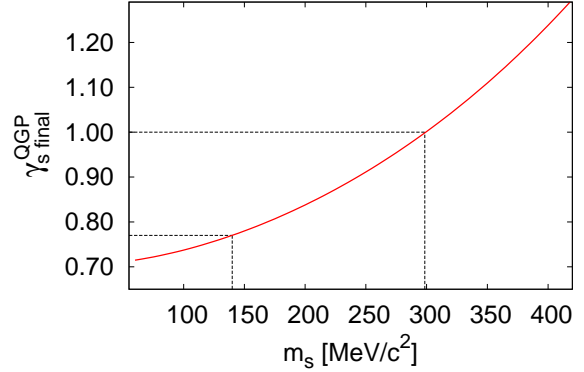


Figure 5. (color online) The strangeness phase space occupancy in the QGP phase as defined by Eq. (2) and correlated in the fit to strangeness density with the strange quark mass. See text.

helps to distinguish from that in the hadron phase where we used γ_s without a superscript. The degeneracy $g = 12 = 2_{\text{spin}} 3_{\text{color}} 2_p$ where the last factor accounts for the presence of both quarks and antiquarks. We will discuss below the reduction in s due to color-interactions.

In central LHC collisions, the large volume (longer lifespan) suggests that strangeness approaches saturated yield in the QGP. This hypothesis is confirmed by almost constant particle ratios we discussed above, see Figure 4. However, in peripheral collisions, the short lifespan of the fireball may not be sufficient to reach chemical equilibrium. Therefore we introduce a centrality dependent strangeness phase space occupancy $\gamma_s^{\text{QGP}}(N_{\text{part}})$ which is to be used in Eq.(1).

To model the centrality dependence of $\gamma_s^{\text{QGP}}(N_{\text{part}})$, we recall that the lifespan τ of the fireball depends on the transverse surface of the fireball and hence the time is proportional to the transverse radius $\tau \propto r_{\perp}$. The transverse radius is related to number of participants as $r_{\perp} \propto N_{\text{part}}^{1/3}$. Thus, at mid-rapidity, the strangeness production will be assumed to be proportional to $r_{\perp}^2 \propto N_{\text{part}}^{2/3}$ and modeled by the usual saturating functional form:

$$\gamma_s^{\text{QGP}}(N_{\text{part}}) = \gamma_{s \text{ final}}^{\text{QGP}} \tanh \left[\left(\frac{N_{\text{part}}}{N_0} \right)^{2/3} \right]. \quad (2)$$

$\gamma_{s \text{ final}}^{\text{QGP}}$ is the asymptotic saturation of strangeness phase space in the QGP for large systems and N_0 controls the scale of the fireball transverse size.

We now match the strangeness density measured in the hadron phase shown in Figure 3 with the centrality dependent strangeness density in the QGP, using Eq.(2) in Eq.(1). Our fit to the observed strangeness density is shown in Figure 3. We observe a very strong correlation between m_s and $\gamma_{s \text{ final}}^{\text{QGP}}$, which we show as a function in Figure 5, while choosing the best N_0 which converges within a narrow interval of $N_0 \in (11, 14)$. This shows a quick saturation of $\gamma_s^{\text{QGP}}(N_{\text{part}})$, which reaches $0.95 \gamma_{s \text{ final}}^{\text{QGP}}$ already for $N_{\text{part}} \simeq 2N_0 = 30$.

To choose a set of values of $(m_s, \gamma_{s \text{ final}}^{\text{QGP}})$ we consider two cases shown in Figure 5:

- (i) The strangeness in QGP is chemically equilibrated in central collisions, $\gamma_{s \text{ final}}^{\text{QGP}} \simeq 1$. This requires the strange quark to have an effective mass of $m_s = 299 \text{ MeV}/c^2$ at hadronization;
- (ii) We assume the PDG value of strange quark mass [5] $m_s \simeq 140 \text{ MeV}/c^2$ at a scale of $\mu \simeq 2\pi T \simeq 0.9 \text{ GeV}$. This requires $\gamma_{s \text{ final}}^{\text{QGP}} \simeq 0.77$.

We believe that both approaches can coincide in an improved theoretical description:

- (i) We omitted in Eq. (1) the thermal QCD prefactor which reduces the expected QGP strangeness density due to thermal QCD many body interactions. The typical reduction of s is by a factor $(1 - c\alpha_s/\pi)$. With $\alpha_s \simeq 0.65$ and $c \simeq 1$ this effect reduces the QGP density by $\simeq 20\%$. The resultant $\gamma_{s\text{final}}^{\text{QGP}}$ can be 20% larger. This effect is present; we do not know its exact magnitude.
- (ii) The measured value of s could be reduced from hadronization value by longitudinal dilution of strangeness during matter expansion after hadronization. This effect vanishes in the limit of Bjorken scaling as for every particle that moves out, another particle moves back into the central rapidity acceptance domain. The rapidity plateau has not been demonstrated experimentally for strange hadrons at LHC.

We note that longitudinal dilution by 15% restores strangeness abundance to prior expectations [14]. Both effects would allow $m_s \simeq 140 \text{ MeV}/c^2$ to be consistent with $\gamma_{s\text{final}}^{\text{QGP}} \simeq 1$.

4. Conclusions

The most important result of this analysis is complete stability at 1%-level of results presented in Ref. [1]. This earlier analysis is fully compatible with the latest results [3, 4]. The 1–1.5 s.d. discrepancy of Λ yield systematically below the experimental result inspired us to explore potential Λ sources. We investigated the finite width of all resonances. We found that our fit is very stable and confidence level is slightly improved, however to explain Λ yield we needed the 2-star (**) resonance $\Sigma(1560)$, increasing the model yield of Λ to within $1/2$ s.d. of the experimental yield. $\Sigma(1560)$ causes no other change in the outcome of our analysis.

We then considered in detail how to interpret the strangeness yield present at hadronization in terms of a QGP inspired model. We considered strangeness conservation during hadronization and concluded that for a fully consistent description we must account for possible reduction of s by interactions. We then argued that the relatively low hadronization strangeness density could be a consequence of particle dilution in central rapidity region should Bjorken scaling not apply fully. Hadrons from jet quenching and charm decay are produced predominantly in central rapidity domain.

Acknowledgments

This work has been supported by a grant from the U.S. Department of Energy, grant DE-FG02-04ER41318, Laboratoire de Physique Théorique et Hautes Energies, LPTHE, at University Paris 6 is supported by CNRS as Unité Mixte de Recherche, UMR7589.

References

- [1] M. Petran, J. Letessier, V. Petracek and J. Rafelski, arXiv:1303.2098 [hep-ph].
- [2] M. Petran and J. Rafelski, Phys. Rev. C **88**, 021901 (2013) arXiv:1303.0913 [hep-ph].
- [3] B. Abelev *et al.* [ALICE Collaboration], arXiv:1307.5530 [nucl-ex].
- [4] B. B. ABELEV *et al.* [ALICE Collaboration], arXiv:1307.5543 [nucl-ex].
- [5] J. Beringer *et al.* [Particle Data Group Collaboration], Phys. Rev. D **86**, 010001 (2012).
- [6] G. Torrieri, S. Steinke, W. Broniowski, W. Florkowski, J. Letessier and J. Rafelski, Comput. Phys. Commun. **167**, 229 (2005) [nucl-th/0404083].
- [7] G. Torrieri, S. Jeon, J. Letessier and J. Rafelski, Comput. Phys. Commun. **175**, 635 (2006) [nucl-th/0603026].
- [8] B. T. Meadows, “Hyperons In Production,” In Proceedings *Baryon 1980*, Toronto 1980 pp 283-300
- [9] J. Olmsted *et al.* [Crystal Ball Collaboration], Phys. Lett. B **588**, 29 (2004) [nucl-ex/0308005].
- [10] P. J. Litchfield, Phys. Lett. B **51**, 509 (1974).
- [11] J. Letessier and J. Rafelski, Camb. Monogr. Part. Phys. Nucl. Phys. Cosmol. **18**, 1 (2002).
- [12] M. Petran and J. Rafelski, Phys. Rev. C **82**, 011901 (2010) [arXiv:0912.1689 [hep-ph]].
- [13] K. Aamodt *et al.* [ALICE Collaboration], Phys. Lett. B **696**, 328 (2011) [arXiv:1012.4035 [nucl-ex]].
- [14] J. Rafelski and J. Letessier, Phys. Rev. C **83**, 054909 (2011) [arXiv:1012.1649 [hep-ph]].